



Design, synthesis, and apoptotic antiproliferative action of new 1,2,3-triazole/1,2,4-oxadiazole hybrids as dual EGFR/VEGFR-2 inhibitors

Mohamed A. Mahmoud, Anber F. Mohammed, Ola I. A. Salem, Tahani Mazyad Almutairi, Stefan Bräse & Bahaa G. M. Youssif

To cite this article: Mohamed A. Mahmoud, Anber F. Mohammed, Ola I. A. Salem, Tahani Mazyad Almutairi, Stefan Bräse & Bahaa G. M. Youssif (2024) Design, synthesis, and apoptotic antiproliferative action of new 1,2,3-triazole/1,2,4-oxadiazole hybrids as dual EGFR/VEGFR-2 inhibitors, *Journal of Enzyme Inhibition and Medicinal Chemistry*, 39:1, 2305856, DOI: [10.1080/14756366.2024.2305856](https://doi.org/10.1080/14756366.2024.2305856)

To link to this article: <https://doi.org/10.1080/14756366.2024.2305856>



© 2024 The Author(s). Published by Informa UK Limited, trading as Taylor & Francis Group.



[View supplementary material](#)



Published online: 07 Feb 2024.



[Submit your article to this journal](#)



Article views: 349



[View related articles](#)



[View Crossmark data](#)

RESEARCH ARTICLE



Design, synthesis, and apoptotic antiproliferative action of new 1,2,3-triazole/1,2,4-oxadiazole hybrids as dual EGFR/VEGFR-2 inhibitors

Mohamed A. Mahmoud^a, Anber F. Mohammed^a, Ola I. A. Salem^a, Tahani Mazyad Almutairi^b, Stefan Bräse^c and Bahaa G. M. Youssif^a

^aPharmaceutical Organic Chemistry Department, Faculty of Pharmacy, Assiut University, Assiut, Egypt; ^bDepartment of Chemistry, College of Science, King Saud University, Riyadh, Saudi Arabia; ^cInstitute of Biological and Chemical Systems, IBCS-FMS, Karlsruhe Institute of Technology, Karlsruhe, Germany

ABSTRACT

A novel series of 1,2,3-triazole/1,2,4-oxadiazole hybrids (**7a–o**) was developed as dual inhibitors of EGFR/VEGFR-2. Compounds **7a–o** were evaluated as antiproliferative agents with Erlotinib as the reference drug. Results demonstrated that most of the tested compounds showed significant antiproliferative action with GI_{50} values ranging from 28 to 104 nM, compared to Erlotinib ($GI_{50} = 33$ nM), and compounds **7i–m** were the most potent. Compounds **7h**, **7i**, **7j**, **7k**, and **7l** were evaluated as dual EGFR/VEGFR-2 inhibitors. These *in vitro* experiments demonstrated that compounds **7j**, **7k**, and **7l** are potent antiproliferative agents that may operate as dual EGFR/VEGFR-2 inhibitors. Compounds **7j**, **7k**, and **7l** were evaluated for their apoptotic potential activity, where findings indicated that compounds **7j**, **7k**, and **7l** promote apoptosis by activating caspase-3, 8, and Bax and down-regulating the anti-apoptotic Bcl-2. Molecular docking simulations show the binding mode of the most active antiproliferative compounds within EGFR and VEGFR-2 active sites.

ARTICLE HISTORY

Received 3 October 2023
Revised 7 December 2023
Accepted 7 January 2024

KEYWORDS

Triazole; oxadiazole; EGFR; VEGFR-2; apoptosis; antiproliferative

Introduction

Despite enormous efforts over the last two decades to find effective therapies, cancer remains a menace to the globe today¹. While conventional cancer treatments cannot distinguish between healthy and malignant cells, targeted therapy kills cancer cells while preserving healthy cells by disrupting critical metabolic pathways or oncoproteins required for tumour cell growth and survival^{1,2}.

Protein tyrosine kinases are important in signal transduction pathways that govern cellular processes such as proliferation, differentiation, migration, and angiogenesis^{3,4}. The epidermal growth factor receptor (EGFR) is a type of membrane receptor tyrosine kinase that is overexpressed in various tumours. Because EGFR tyrosine kinase signal transduction is closely linked to tumour progression, inhibiting receptor activity can effectively inhibit tumours^{5–7}. Another significant receptor tyrosine kinase that can induce angiogenesis is vascular endothelial growth factor receptor (VEGFR-2)⁸. VEGFR-2, a VEGFR family member, is a major mediator in tumour angiogenesis and is essential for solid tumour formation. Inhibiting VEGFR-2 has been proposed as an effective method for preventing angiogenesis^{9,10}.

VEGFR-2 and EGFR have been identified as promising therapeutic targets for cancer treatment. They are essential in the signalling pathways that regulate tumour cell proliferation, differentiation, migration, and angiogenesis^{11–14}. EGFR and VEGFR-2 typically share common downstream signalling pathways as a complex signal network of interconnected circuits. EGFR inhibition

can reduce VEGF expression and attenuate angiogenesis while increasing VEGFR-2 expression, eventually leading to EGFR inhibitor resistance^{15,16}. As a result, inhibiting both EGFR and VEGFR-2 simultaneously has become an effective cancer therapeutic strategy with a synergistic impact^{17–19}.

The 1,2,4-oxadiazole heterocycle has been widely studied over the last four decades, yielding many analogs with diverse biological effects. Due to the potential for particular interactions (such as hydrogen bonding), the 1,2,4-oxadiazole achieves bioisosteric equivalence with amide and ester moieties^{20,21}. The 1,2,4-oxadiazole nucleus is the basic core of a number of drugs on the market today, including Oxolamine, Butalamine, Prenoxdiazine, Fasiplon, and Proxazole^{22–24}. A new series of 1,2,4-oxadiazole-based compounds was developed and tested as anticancer agents that target the EGFR inhibitory pathway. The optimal derivative was compound **I** (Figure 1), demonstrating equipotent antiproliferative action against a panel of five NSCLC cell lines ($IC_{50} = 0.2–0.6$ μ M). Cell cycle investigations demonstrated that **I**'s antiproliferative activity is linked to its ability to cause G2/M arrest and, to a lesser extent, apoptosis²⁵.

Saritha et al.²⁶ reported on the design, synthesis, and antiproliferative efficacy of a new series of molecular hybrids containing benzimidazole, thiazolidine-2,4-dione, and 1,2,4-oxadiazole scaffolds against three human cancer cell lines, MCF-7, A-549, and HepG2. Compound (**II**, Figure 1) demonstrated greater activity against all cell lines, with the highest activity against MCF-7 ($IC_{50} =$

CONTACT Stefan Bräse  braese@kit.edu  Institute of Biological and Chemical Systems, IBCS-FMS, Karlsruhe Institute of Technology, 76131 Karlsruhe, Germany; Bahaa G. M. Youssif  bgyoussif2@gmail.com; bahaa.youssif@pharm.aun.edu.eg; bgyoussif@ju.edu.sa  Pharmaceutical Organic Chemistry Department, Faculty of Pharmacy, Assiut University, Assiut 71526, Egypt.

This article has been corrected with minor changes. These changes do not impact the academic content of the article.

 Supplemental data for this article can be accessed [here](#).

© 2024 The Author(s). Published by Informa UK Limited, trading as Taylor & Francis Group.

This is an Open Access article distributed under the terms of the Creative Commons Attribution-NonCommercial License (<http://creativecommons.org/licenses/by-nc/4.0/>), which permits unrestricted non-commercial use, distribution, and reproduction in any medium, provided the original work is properly cited. The terms on which this article has been published allow the posting of the Accepted Manuscript in a repository by the author(s) or with their consent.

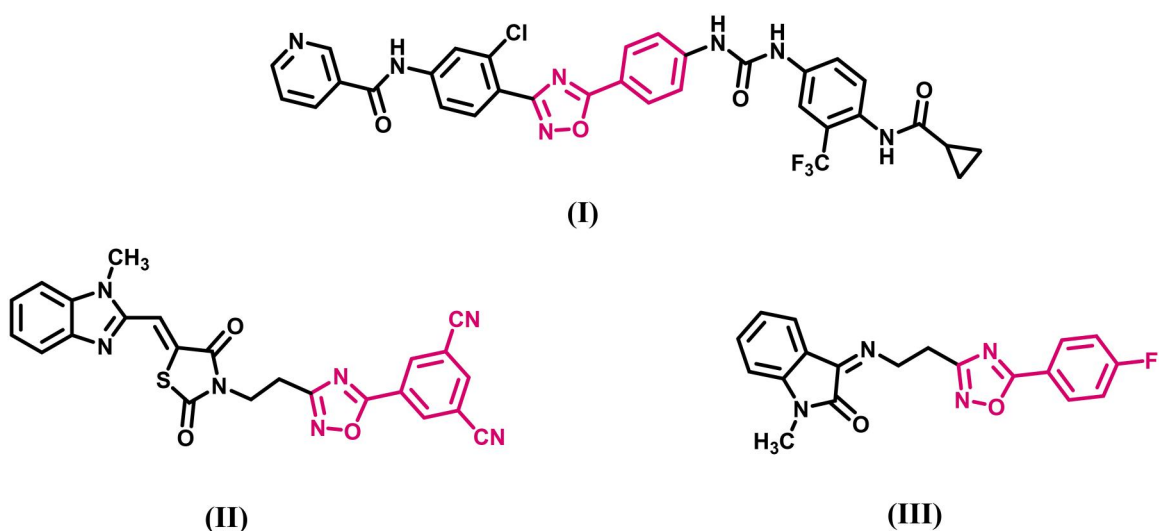


Figure 1. Structure of anticancer 1,2,4-oxadiazoles I-III.

$1.32 \pm 0.05 \mu\text{M}$) as compared to the reference Erlotinib ($\text{IC}_{50} = 4.15 \pm 0.12 \mu\text{M}$). Similarly, new isatin-1,2,4-oxadiazole hybrids were produced and tested for cytotoxicity against four human cancer cell lines. Their potential VEGFR-2 inhibition assay was also investigated, with compound (III, Figure 1) having nearly double the inhibitory potency as Sorafenib, with $\text{IC}_{50} = 35.64 \pm 1.56 \text{ nM}$ against VEGFR-2 enzyme assay.

In a recent publication²⁷, we describe the discovery of a new series of 1,2,3-triazole-based antiproliferative agents, compounds **6a-o** (Figure 2). The newly synthesised compounds were tested for antiproliferative activity against a panel of four cancer cell lines, with compound **6k** ($\text{R} = 3,4\text{-di-OMe}$) being the most potent derivative with a GI_{50} value of 31 nM against the tested four cancer cell lines, outperforming the reference Erlotinib ($\text{GI}_{50} = 33 \text{ nM}$). The EGFR and VEGFR-2 inhibitory assay results showed that compound **6k** ($\text{R} = 3,4\text{-di-OMe}$), the most potent antiproliferative agent, was also the most potent anti-EGFR and anti-VEGFR-2 agent, with IC_{50} values of 83 ± 05 and $1.80 \pm 0.05 \text{ nM}$, respectively, compared to Erlotinib ($\text{IC}_{50} = 80 \pm 4 \text{ nM}$) and Sorafenib ($\text{IC}_{50} = 0.17 \pm 0.01 \text{ nM}$).

Motivated by previous findings and in pursuit of a new antiproliferative agent with dual or multi-targeted inhibitory action²⁷⁻³⁰, we present here the design, synthesis, and antiproliferative activity of a novel series of 1,2,3-triazole/1,2,4-oxadiazole hybrids (**7a-o**, Figure 2) as dual EGFR/VEGFR-2 inhibitors. The newly designed 1,2,4-oxadiazoles **7a-o** were considered to be sterically fixed counterparts of the previously discovered linear carboximidamide derivatives **6a-o** (Figure 2). Such a rigid conformation may result in tight fitting within the EGFR and VEGFR-2 active sites, increasing the efficacy of newly synthesised compounds. The antiproliferative effect of compounds **7a-o** against four cancer cell lines was investigated using Erlotinib as the reference drug. Next, the most effective compounds were evaluated for inhibitory action against EGFR and VEGFR-2, which were identified as possible targets for their action. In addition, the apoptotic potential of the most active compounds was assessed. Finally, docking analysis and ADME studies were performed for the most potent derivatives.

Results and discussion

Chemistry

Scheme 1 outlines the synthetic steps for the target compounds **7a-o**. Compound **1** was hydrolysed in aqueous NaOH (20%) and

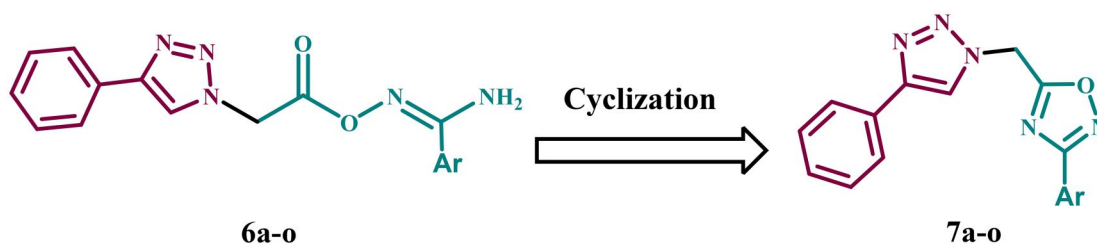
refluxed for two hours to produce compound **2**³¹. On the other hand, compounds **4a-o** were prepared according to a reported procedure in THF *via* an iodine-catalyzed transformation of the formyl group in **3a-o** to a cyano group utilising ammonia as a nitrogen source³². Amidoximes **5a-o** were prepared in THF by nucleophilic attack of hydroxylamine at the cyanide carbon of **4a-o**³³. Aryl carboximidamides **6a-o** were prepared by reacting carboxylic acid **2** with the appropriate amidoximes **5a-o** in dry acetonitrile using the activating agent *N,N'*-carbonyl diimidazole (CDI)²⁷.

Reagents and reaction conditions: (a) 20% aq. NaOH, reflux, 2 h, 80%; (b) 33% aq. NH_3 , THF, I_2 , r.t 3–5 h, 40–85%; (c) $\text{NH}_2\text{OH}\cdot\text{HCl}$, Na_2CO_3 , methanol, reflux, 6–8 h; (d) CDI, dry CH_3CN , r.t 10 h; (e) CH_3CN , reflux, overnight, 46–90%.

The target compounds **7a-o** were synthesised by refluxing the appropriate carboximidamides **6a-o** in dry acetonitrile. After the reaction was completed (as monitored by TLC), the excess solvent evaporated under reduced pressure. The precipitates were washed with cold water and filtered, crystallised from acetonitrile to yield 1,2,4-oxadiazoles **7a-o** in good yields.

The structures of new compounds **7a-o** were elucidated using NMR, IR, and elemental microanalysis. FTIR spectra of target compounds **7a-o** confirmed the disappearance of (NH_2) and ($\text{C}=\text{O}$) peaks of the precursor aryl carboximidamides **6a-o**. The presence of (CH) peaks at 3144, 3001, 2965 cm^{-1} , ($\text{C}=\text{N}$ and $\text{C}=\text{C}$) peaks at 1602, 1579, 1468 cm^{-1} , and ($\text{Ar}-\text{CH}$ bending) at 856 cm^{-1} in the FTIR spectrum of compound **7g** as a representative example verified the prior observations.

Also, ^1H NMR spectra proved the cyclisation reaction by revealing the absence of amino (NH_2) wide signals in compounds **6a-e** and the appearance of ($\text{N}-\text{CH}_2$) signals at ($\delta = 6.37\text{--}6.14 \text{ ppm}$) compared with compounds' **6a-o** ($\text{N}-\text{CH}_2$) signals that appeared in the range of ($\delta = 6.66\text{--}5.61 \text{ ppm}$). ^1H NMR spectrum of compound **7g** confirmed the elucidated structure by showing a singlet triazole C–H signal at $\delta = 8.82 \text{ ppm}$, and nine aromatic protons appeared as five distinct signals in the aromatic region. Moreover, ^{13}C NMR spectra confirmed the cyclisation reaction by the disappearance of the $\text{C}=\text{O}$ signal of their precursors **6a-o** at $\delta = 166 \text{ ppm}$ and the appearance of ($\text{N}-\text{CH}_2$) signal at ($\delta = 45.6\text{--}45 \text{ ppm}$). ^{13}C NMR spectrum of compound **7g** confirmed the elucidated structure by the appearance of 12 aromatic signals at $\delta = 175.1\text{--}122.9$, CF_3 quartette signal at $\delta = 124$ with $J = 272.7 \text{ Hz}$, and $\text{N}-\text{CH}_2$ signal as $\delta = 45.3 \text{ ppm}$.



Compd.	Ar	Compd.	Ar
6a, 7a		6h, 7h	
6b, 7b		6i, 7i	
6c, 7c		6j, 7j	
6d, 7d		6k, 7k	
6e, 7e		6l, 7l	
6f, 7f		6m, 7m	
6g, 7g		6n, 7n	
		6o, 7o	

Figure 2. Structures of previously reported compounds 6a–o and newly synthesised 7a–o.

Biology

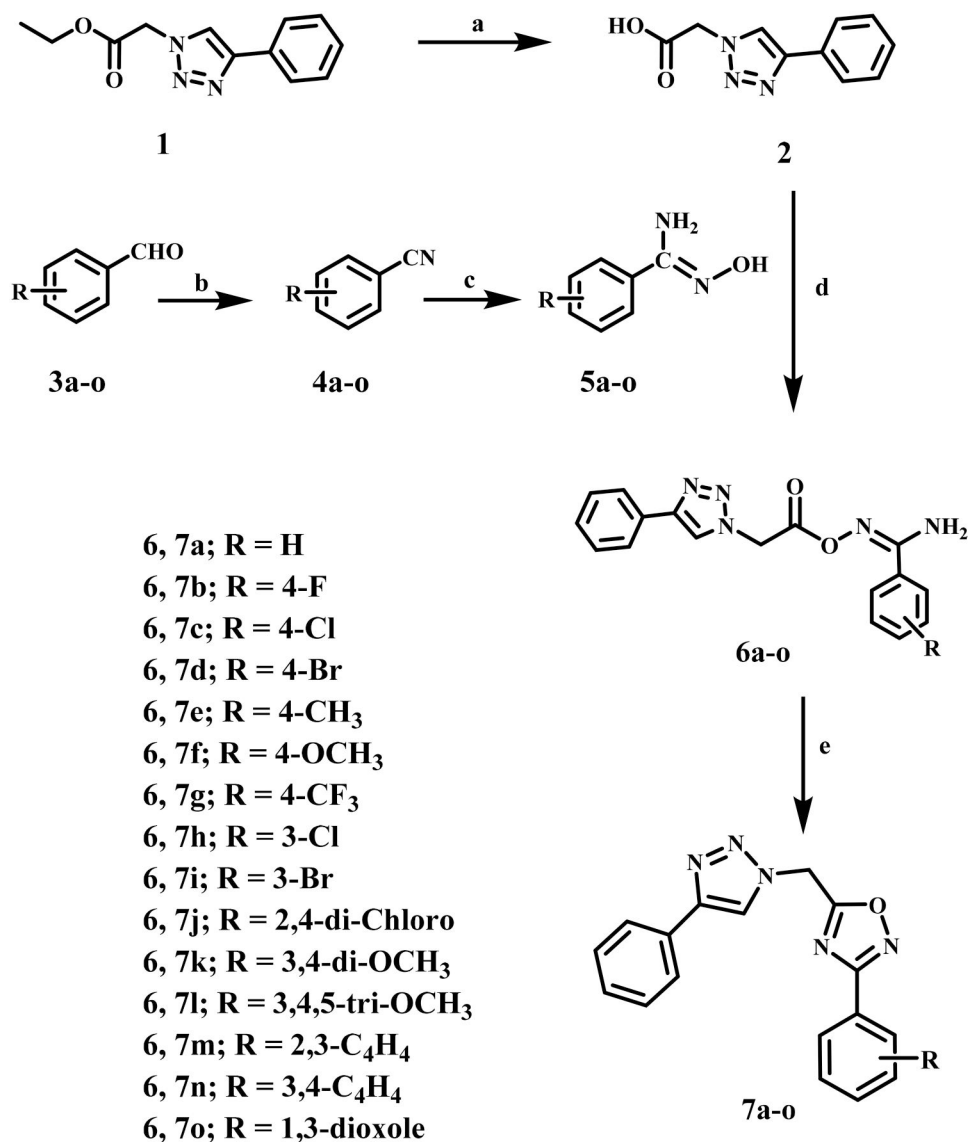
Cell viability assay

A cell viability experiment was performed on the MCF-10A (normal human mammary gland epithelial) cell line to assess the effect of compounds 7a–o on normal cell lines^{34,35}. Before testing cell viability, 50 μ M of the examined compound is used in this investigation for

four days. Compounds 7a–o have no cytotoxic impact and are greater than 87% cell viability, as shown in Table 1.

Antiproliferative assay

The antiproliferative activity of 1,2,4-oxadiazoles 7a–o was evaluated against four different human cancer cell lines, namely, colon



Scheme 1. Synthetic pathway of compounds 7a-o

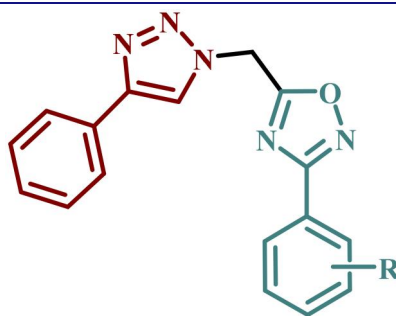
cancer (HT-29) cell line, lung cancer (A-549) cell line, pancreatic cancer (Panc-1) cell line, and breast cancer (MCF-7) cell line using Erlotinib as the reference drug^{36,37}. The median inhibitory concentration (IC₅₀) is shown in Table 1. The results showed that the tested compounds **7a-o** had promising antiproliferative action with GI₅₀ values ranging from 28 to 104 nM. The six most active derivatives were **7h-m**, with GI₅₀ values ranging from 28 to 45 nM, compared to Erlotinib's 33 nM.

Compound **7l** (R=3,4,5-tri-Ome) was the most potent derivative, with a GI₅₀ value of 28 nM against the four cancer cell lines examined, outperforming the reference Erlotinib (GI₅₀ = 33 nM). Compound **7l** was shown to be more potent than Erlotinib against all four human cancer cell lines examined. Compound **7k** (R=3,4-dimethoxy) scored second in activity against the four cancer cell lines with a GI₅₀ value of 32 nM, equipping to the reference Erlotinib (GI₅₀ = 33 nM). Compound **7k** was more potent than Erlotinib against the breast cancer (MCF-7) cell line, having an IC₅₀ value of 35 ± 3 nM versus 40 ± 3 nM for Erlotinib. According to the results of compounds **7f** (R=4-OMe) and **7k** (R=3,4-di-OMe), the number of methoxy groups substantially impacts the activity of these compounds. Compounds **7f** (R=4-OMe) and **7k** (R=3,4-di-OMe) were less potent than compound **7l** (R=3,4,5-tri-

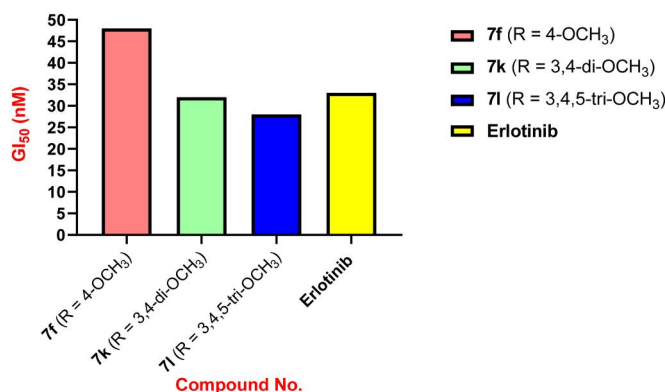
OMe), indicating that the trimethoxy groups were best suited for antiproliferative action, Figure 3.

Compound **7j** (R=2,4-di-Cl) was the third most active against the four cancer cell lines, with a GI₅₀ value of 35 nM. Compound **7j** was likewise more potent than Erlotinib against the breast cancer (MCF-7) cell line, with an IC₅₀ value of 36 ± 3 nM versus Erlotinib's IC₅₀ of 40 ± 3 nM. Another key point drawn from the findings in Table 1 is the effect of halogen atom type, position, and number on antiproliferative activity. Compounds **7b** (R=4-F), **7c** (R=4-Cl), **7d** (R=4-Br), **7i** (R=3-Br), and **7h** (R=3-Cl) demonstrated good antiproliferative action with GI₅₀ values ranging from 37 to 104 nM, being less potent than compound **7j** (R=2,4-di-Cl) indicating that the number of halogen atoms had a significant impact on the antiproliferative action of these compounds and that dihalo derivatives are more potent than mono halo substituted derivatives.

Compounds **7i** (R=3-Br) and **7h** (R=3-Cl) demonstrated significant antiproliferative activity, with GI₅₀ values of 37 and 42 nM, respectively, demonstrating that the bromine atom is better tolerated for antiproliferative action than the chlorine atom. Furthermore, compounds **7c** (R=4-Cl) and **7d** (R=4-Br) had weak antiproliferative activity, with GI₅₀ values of 90 nM and 82 nM,

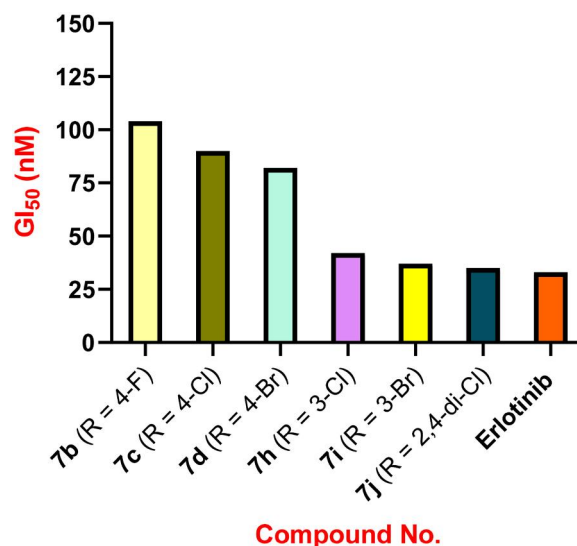
Table 1. Antiproliferative activity of compounds **7a–o** and Erlotinib.**7a-o**

Comp.	Cell viability% (50 μ M)	R	Antiproliferative activity $IC_{50} \pm SEM$ (nM)					Average (GI_{50})
			A-549	MCF-7	Panc-1	HT-29		
7a	90	H	94 \pm 9	98 \pm 9	96 \pm 9	96 \pm 9	96	
7b	91	4-F	102 \pm 10	106 \pm 10	104 \pm 10	104 \pm 10	104	
7c	89	4-Cl	87 \pm 8	94 \pm 9	90 \pm 9	92 \pm 9	90	
7d	88	4-Br	80 \pm 8	84 \pm 8	80 \pm 8	82 \pm 8	82	
7e	91	4-CH ₃	98 \pm 9	102 \pm 9	100 \pm 10	102 \pm 10	101	
7f	90	4-OMe	48 \pm 4	51 \pm 5	48 \pm 4	46 \pm 4	48	
7g	87	4-CF ₃	66 \pm 6	68 \pm 6	68 \pm 6	66 \pm 6	67	
7h	90	3-Cl	40 \pm 4	44 \pm 4	40 \pm 4	42 \pm 4	42	
7i	89	3-Br	36 \pm 3	39 \pm 3	37 \pm 3	37 \pm 3	37	
7j	91	2,4-Di-Cl	33 \pm 3	36 \pm 3	34 \pm 3	36 \pm 3	35	
7k	89	3,4-Di-OMe	30 \pm 3	35 \pm 3	32 \pm 3	32 \pm 3	32	
7l	88	3,4,5-Tri-OMe	26 \pm 2	30 \pm 3	28 \pm 2	28 \pm 2	28	
7m	87	2,3-C ₄ H ₄	42 \pm 4	48 \pm 4	46 \pm 4	44 \pm 4	45	
7n	89	3,4-C ₄ H ₄	68 \pm 6	74 \pm 7	70 \pm 7	72 \pm 7	71	
7o	91	1,3-Dioxole	74 \pm 7	80 \pm 8	78 \pm 7	76 \pm 7	77	
Erlotinib	–	–	30 \pm 3	40 \pm 3	30 \pm 3	30 \pm 3	33	

**Figure 3.** GI_{50} of compounds **7f**, **7k**, and **7l** compared to Erlotinib.

respectively, approximately twice as weak as the 3-halosubstituted derivatives **7i** and **7h**. Finally, with a GI_{50} value of 104 nM, the 4-fluoro derivative **7b** (R = 4-F) was the least potent of all synthesized derivatives, 2.5-fold less active than the 3-halo-substituted derivatives **7i** and **7h**. These findings indicated that the type, position, and number of halogen atoms had a significant effect on antiproliferative activity, with activity increasing in the order 2,4-di-Cl > 3-Br > 3-Cl > 4-Br > 4-Cl > 4-F, **Figure 4**.

The antiproliferative impact of the 1-naphthyl derivative **7m** (R = 2,3-C₄H₄) was promising, with a GI_{50} value of 45 nM, which was 1.4-fold less potent than the reference Erlotinib (GI_{50} = 33 nM). On the other hand, the 2-naphthyl derivative **7n** (R = 3,4-C₄H₄)

**Figure 4.** GI_{50} of compounds **7b**, **7c**, **7d**, **7h**, **7i**, **7j** and Erlotinib.

demonstrated weak antiproliferative activity with a GI_{50} value of 77 nM, being 2.4-fold and 1.7-fold less potent than Erlotinib and the 1-naphthyl derivative **7m**, respectively.

The unsubstituted derivative, compound **7a** (R = H), and the 4-methyl derivative **7e** (R = 4-CH₃) were 3-fold less potent than the reference Erlotinib, with GI_{50} values of 96 and 101 nM, respectively,

demonstrating the effect of the substitution pattern on the phenyl ring of the 1,2,4-oxadiazole moiety.

EGFR inhibitory assay

The inhibitory effects of the most potent antiproliferative derivatives **7h–l** on EGFR, as a possible target for their antiproliferative action, were investigated using Erlotinib as the reference drug^{28,38}. Table 2 shows the results as IC₅₀ values.

Generally, compounds **7h–l** displayed potential anti-EGFR action, with IC₅₀ values ranging from 76 to 105 nM. The results of this cell-based experiment are consistent with those of the antiproliferative assay, in which the most potent antiproliferative agent, **7l** (R = 3,4,5-tri-OMe), was also the most potent anti-EGFR, with an IC₅₀ value of 76 ± 06 nM, exceeding the reference Erlotinib, which had an IC₅₀ value of 80 ± 05 nM. Compounds **7k** (R = 3,4-dimethoxy) and **7j** (R = 2,4-di-Cl) were placed second and third in EGFR inhibitory activity, with IC₅₀ values of 82 and 89 nM, respectively, and were comparable to the reference Erlotinib.

These findings highlighted the significance of the methoxy group and the number of chlorine atoms in antiproliferative and anti-EGFR activities. Compounds **7h** (R = 3-Cl) and **7i** (R = 3-Br) displayed moderate anti-EGFR activity, with IC₅₀ values of 105 ± 10 and 97 ± 9 nM, respectively, and were found to be less potent than the reference Erlotinib, which had an IC₅₀ value of 80 ± 05. These findings indicated that derivatives **7j**, **7k**, and **7l**, which require additional structural modifications to develop more potent derivatives, may be capable of inhibiting cancer cell proliferation by targeting the EGFR.

VEGFR inhibitory assay

The inhibitory efficacy of compounds **7h–l** against VEGFR-2 was determined by applying kinase-glo-luminescent kinase assays with Sorafenib as the control medication³⁹. Table 2 displays the results as IC₅₀ values.

The results showed that the investigated compounds inhibited VEGFR-2 significantly, with IC₅₀ values ranging from 2.40 to 6.90 nM, compared to Sorafenib, which had an IC₅₀ value of 0.17 nM. The most potent derivatives were **7j**, **7k**, and **7l**, with IC₅₀ values of 2.40, 3.80, and 4.70 nM, respectively. Again,

Table 2. IC₅₀ values of compounds **7h**, **7i**, **7j**, **7k**, **7l**, Erlotinib and Sorafenib against EGFR and VEGFR-2.

Compd. no.	EGFR inhibition IC ₅₀ ± SEM (nM)	VEGFR-2 inhibition IC ₅₀ ± SEM (nM)
7h	105 ± 10	6.90 ± 0.07
7i	97 ± 09	5.50 ± 0.05
7j	89 ± 08	4.70 ± 0.04
7k	82 ± 07	3.80 ± 0.03
7l	76 ± 06	2.40 ± 0.02
Erlotinib	80 ± 05	–
Sorafenib	–	0.17 ± 0.01

–, not determined.

Table 3. Caspase-3, caspase-8, Bax, and Bcl-2 levels of compounds **7j**, **7k**, and **7l**.

Compd. no.	Caspase-3		Caspase-8		Bax		Bcl-2	
	Conc (Pg/mL)	Fold change	Conc (ng/mL)	Fold change	Conc (Pg/mL)	Fold change	Conc (ng/mL)	Fold reduction
7j	460 ± 4	7.0	2.00	22	291	32	0.95	5
7k	530 ± 5	8.0	2.30	25	310	34	0.80	6
7l	587 ± 5	9.0	2.55	28	362	40	0.60	8
Staurosporine	465 ± 4	7.0	1.85	21	288	32	1.00	5
Control	65	1.0	0.09	1	9	1	5.00	1

compound **7l** was the most potent derivative as a VEGFR-2 inhibitor, with an IC₅₀ value of 2.40 ± 0.02 nM. These findings demonstrate that compounds **7j**, **7k**, and **7l** are potent antiproliferative agents that may act as dual EGFR/VEGFR-2 inhibitors.

Apoptosis assay

Cancer can be treated by regulating or stopping the uncontrolled multiplication of cancer cells. Using the cell's natural dying process is a highly effective method. Apoptosis evasion is a trait of cancer and is not specific to the aetiology or kind of cancer; hence, targeting apoptosis is useful for many types of cancer. Many anticancer drugs target various stages of both the intrinsic and extrinsic pathways^{40–42}. Compounds **7j**, **7k**, and **7l**, the most potent derivatives in all *in vitro* studies, were tested for their capacity to initiate the apoptosis cascade and reveal their proapoptotic potential.

Caspase-3 activation assay

Caspases are vital for the induction and maintenance of apoptosis. Caspase-3 is an essential caspase that cleaves many cell proteins, causing apoptosis^{43,44}. Compounds **7j**, **7k**, and **7l** were investigated as caspase-3 activators against the human epithelial (A-594) cancer cell line⁴⁵, and the findings are shown in Table 3.

Compounds **7k** and **7l** showed a promising increase in caspase-3 protein levels of up to 530 ± 5 and 587 ± 5 pg/mL, respectively. They increased caspase 3 protein levels in the A-594 cancer cell line by 8- and 9-fold compared to untreated control cells. Compounds **7k** and **7l** were more active than the Staurosporine control, which exhibited 465 ± 4 pg/mL caspase-3 overexpression. Compound **7j** was the least active derivative, with a caspase-3 overexpression of 460 ± 4 pg/mL and was comparable to the reference Staurosporine as a caspase-3 level inducer. According to these results, the examined compounds **7j**, **7k**, and **7l** may have apoptotic potential activity, which may account for their antiproliferative effects.

Caspase-8, Bax, and Bcl-2 levels assays

Using Staurosporine as a control, the effects of compounds **7j**, **7k**, and **7l** on the levels of caspase-8, Bax, and the anti-apoptotic protein Bcl-2 against the A-594 cancel cell line were further examined. Table 3 presents the results.

Table 3 demonstrated that compound **7l** (2.55 ng/mL) had the highest levels of caspase-8 overexpression, followed by compound **7k** (2.30 ng/mL) and finally compound **7j** (2.00 ng/mL) when compared to the reference Staurosporine (1.85 ng/mL). The investigated compounds **7j**, **7k**, and **7l** elevated caspase-8 levels by 22, 25, and 28 times, respectively, compared to the untreated control cell.

Furthermore, compounds **7k** and **7l** boosted Bax induction 34- and 40-fold (310 and 362 pg/mL, respectively) over untreated A-

594 cancer cells, outperforming Staurosporine (288 pg/mL, a 32-fold induction), while compound **7j**, on the other hand, induces Bax at a level comparable to Staurosporine. They were finally compared to Staurosporine, derivatives **7j**, **7k**, and **7l** significantly reduced anti-apoptotic Bcl-2 protein levels in the A-594 cell line (5-, 6-, and 8-folds, respectively). These data suggest that compounds **7j**, **7k**, and **7l** promote apoptosis by activating caspase-3, 8, and Bax and down-regulating the anti-apoptotic Bcl-2.

Docking study

EGFR active site

In silico docking simulations were performed for the most potent antiproliferative compounds, **7h**, **7i**, **7j**, **7k**, and **7l**, to study their molecular interaction with the epidermal growth factor receptor tyrosine kinase EGFR. Molecular operating environment (MOE) software⁴⁶ was used, as well as the crystal structure of the EGFR in complex with Erlotinib (PDB: 1M17)⁷.

MOE minimizations were performed with the force field (OPLS-AA) using Born solvation. Before simulations, the protein–ligand complex was protonated and corrected. The simulation results of the compounds were compared with Erlotinib, and the data are shown in Table 4. The docking protocol was validated by redocking the co-crystallised ligand into the EGFR binding site, where the docking *S* score obtained for the docked ligand was -10.70 kcal/mol with an *RMSD* value of 1.48 Å.

Concerning docking score analysis, compounds **7k** and **7l** exhibited the highest negative values (-9.52 and -9.57 kcal/mol, respectively), compatible with their *in vitro* EGFR inhibition effects (Table 4). Inspection of the ligand–protein complexes exposed that the ligand–protein interactions were mainly hydrophobic. The new 1,2,4-oxadiazole compounds are sterically fixed analogs of the open carboximidamide derivatives of previous work²⁷. Such a rigid conformation resulted in tight fitting within the EGFR active site with derivatives (R = H, 4-OMe, 3-Cl, 3-Br, 2,4-di-Cl, and 3,4,5-tri-OMe) as the cyclized structure better fits within the bioactive conformation. Compounds **7j**, **7k**, and **7l** adopted an orientation within the large binding site where the phenyl triazole scaffold was inserted deeply into the hydrophobic pocket, aligned with Erlotinib phenyl acetylene moiety. The latter scaffold formed stacking with Phe699 and pi–H interaction with Val702. At the same time, the ligand 2,4-dichloro, 3,4-di-methoxy, or 3,4,5-trimethoxyphenyl moiety directed past the Erlotinib ether linkages at the gate of the binding site. This substituted phenyl moiety formed stacking with Pro770 and pi–H interaction with Leu694 and other hydrophobic interactions with nearby residues Lys721, Asp831, Val702, Leu694, and Gly772.

The trimethoxy derivative **7l** showed the best binding mode and hydrophobic interactions with the surrounding amino acid residues owing to its increased van der Waals volume within the active site relative to the other derivatives (Figure 5C, D). However, the ligand loses H-bond interaction with the key amino acid residue Met769 compared with the H-bond formed by the quinazoline nitrogen of Erlotinib (3.56 Å) (Figure 5E, F). Alternatively, the ligand stabilises its complex by accepting a

strong H-bond from Lys721 in the case of compound **7l** with (3.50 Å) and a weak one from Thr830 in the case of compound **7k** at the hydrophobic hinge (Figure 5A, B).

On the other hand, compounds **7h** and **7i** exhibited another orientation where *m*-chloro and *m*-bromophenyl moiety were better accommodated within the active site than 4-chloro and 4-bromo substituents. The *m*-halophenyl moiety stacked with Phe699 deeply inside the hydrophobic cleft of the enzyme and formed a halogen bond interaction with Leu764 in the case of compound **7i** with (R = *m*-Br). However, the phenyl triazole scaffold formed stacking with Pro770 and pi–H interactions with Cys773 and Gly772 at the gate of the binding site. This indicated that the active site tolerated the *m*-halophenyl rather than the *p*-halophenyl moiety with a bulkier halogen atom (Figure 6).

VEGFR active site

Moreover, the most potent VEGFR-2 inhibitors, **7h**, **7i**, **7j**, **7k**, and **7l**, were docked against vascular endothelial growth factor VEGFR-2. The crystal structure of VEGFR-2 in complex with Sorafenib (PDB: 4ASD)⁴⁷ was used in the present study. The docking protocol was validated by redocking the co-crystallised ligand with an *S* score of -10.73 kcal/mol with an *RMSD* value of 0.46 Å. Again, the trimethoxy compound **7l** showed the highest negative score (-9.10 kcal/mol) among the tested compounds (Table 5). Inspection of the docked complexes revealed that the compounds bind tightly within the binding pocket. Compounds **7l** and **7k** exhibited good fitting (Figure 7A–C), where the phenyl triazole scaffold bi-stacked between Phe918 and Phe92 forming pi–H interaction with Leu840. However, there were missing H-bond interactions with Cys919 at the gate of the binding site. This indicated the significance of introducing an H-bond forming substituent at the phenyl ring to enhance the fitting. On the opposite end of the active site, the dimethoxy or trimethoxy phenyl moiety formed stacking with His1026 and pi–H interaction with Glu885. Interestingly, the oxadiazole moiety accepted a H-bond from Asp1046 and formed pi–H interactions with Phe1047 (**7k**) or Lys868 (**7l**).

Other derivatives showed comparable binding modes within the active site; however, compound **7l** showed the best fitting due to its enhanced van der Waals volume. Results of the docking simulations attributed to investigate the impact of introducing fixed geometry to the open carboximidamide derivatives on the binding modes within active sites and confirm dual EGFR/VEGFR-2 kinase inhibitory effects of compounds **7h**, **7i**, **7j**, **7k**, and **7l**.

Moreover, the most potent compound **7l** adopts DFG-in conformation of active form EGFR as erlotinib forming H-bond with Lys721 at the ATP binding site. However, the compound missed interaction with Asp831 at the DFG sequence. On the other hand, the same compound probes DFG-out conformation of inactive VEGFR-2 forming H-bond with Asp1046 that is equivalent to Asp831 at EGFR. We assumed that this new ligand could act as dual type I/II kinase inhibitor as stabilising DFG-in conformation at EGFR as well as DFG-out conformation at VEGFR-2 and thus could also inhibit phosphorylation, Figure 8.

Table 4. Ligand–protein complex interactions of the tested compounds **7h**, **7i**, **7j**, **7k**, and **7l** within the active site of EGFR.

Compd.	MOE score (kcal/mol)	Hydrogen bond interactions	Hydrophobic interactions	Pi–H interactions
Erlotinib	-10.70	Met769	Leu694, Leu820, Val702, Gly722, Thr766, Thr830	Leu694
7h	-8.18	–	Lys721, Asp831, Val702, Leu820, Leu694, Phe699, Gly772	Gly772, Cys773
7i	-8.45	Leu764	Lys721, Asp831, Leu820, Leu694, Phe699, Gly772	Leu820
7j	-8.77	–	Gly772 Lys721, Asp831, Val702, Leu820, Leu694, Phe699	Gly772, Leu820
7k	-9.52	–	Phe699, Gly772 Lys721, Asp831, Val702, Leu820, Leu694	Gly772
7l	-9.57	Lys721	Leu694, Phe699, Gly772 Lys721, Asp831, Val702, Leu820	Leu694

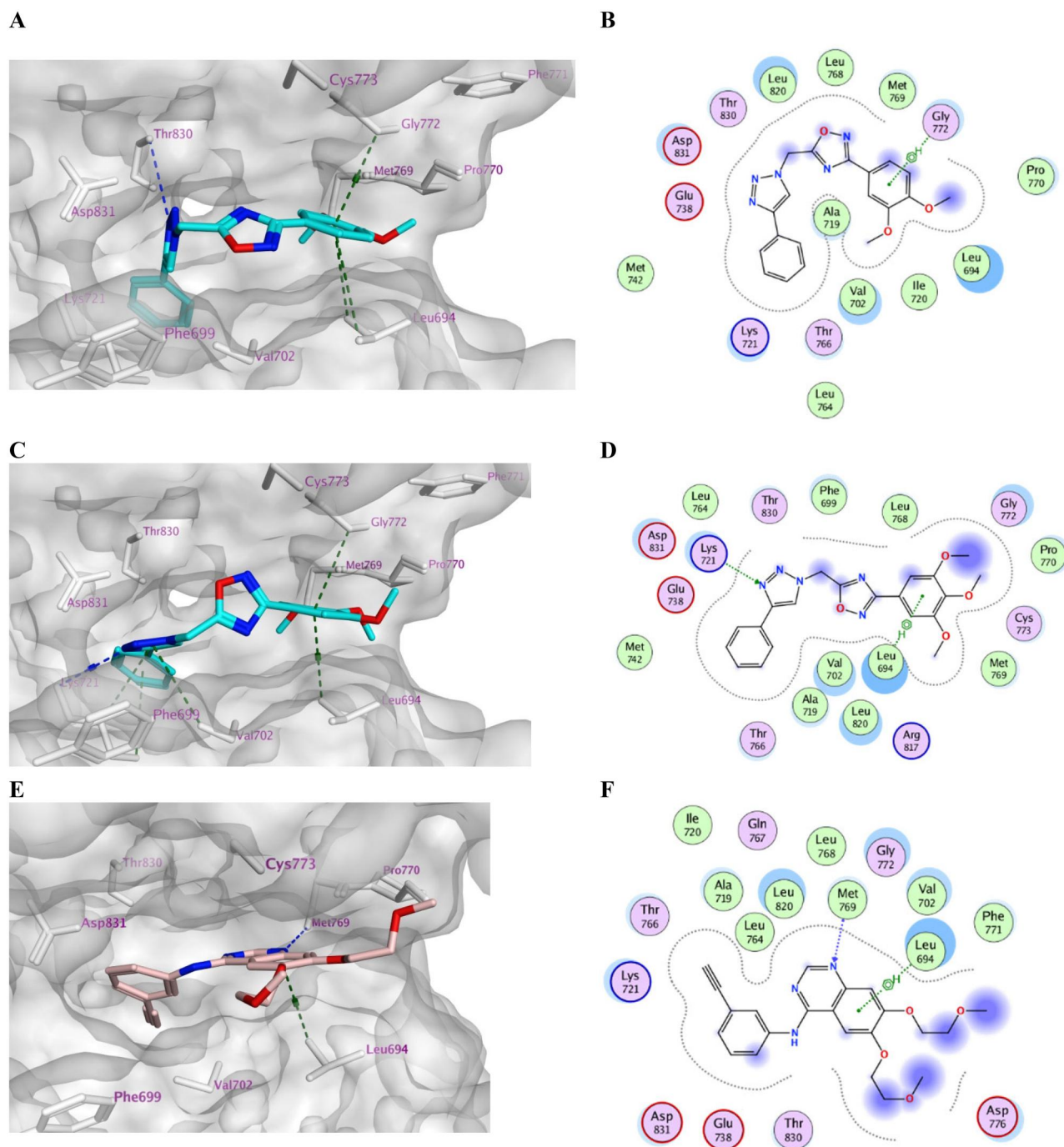


Figure 5. Docking representation models of compound **7k**, **7l**, and Erlotinib within the binding site of EGFR (H-bond: blue dashed lines, Pi-H; green dashed lines). (A) 3D-docked model of compound **7k** (cyan) showing the protein surface (grey); (B) 2D-docked model of compound **7k**; (C) 3D-docked model of compound **7l** (cyan) showing the protein surface (grey); (D) 2D-docked model of compound **7l**; (E) 3D-docked model of compound Erlotinib (pink) showing the protein surface (grey); (F) 2D-docked model of compound Erlotinib.

In silico ADME/pharmacokinetics studies

The most potent antiproliferative 1,2,4-oxadiazole hybrids **7h**, **7i**, **7j**, **7k**, and **7l** were examined for their ADME/Pharmacokinetics properties using the web tool Swiss ADME⁴⁸ by entering a list of the compounds' SMILES (Simplified Molecule Input Line Entry Specification) provided by ChemDraw software.

The *in silico* pharmacokinetic data (Table 6) showed that all 1,2,4-oxadiazole hybrids are orally active as they obey Lipinski's rules of five with zero violation. Also, those hybrids exhibit high intestinal absorbance and are non-substrate for P-gp. None of

those hybrids are likely to cross BBB except **7h**, **7i**, and **7j**. Based on Lipinski's rules, log *P* should be ≤ 5 , 1,2,4-oxadiazole tested hybrids exhibited good permeability as indicated by log *P* values in the range of 2.77–3.85. Amongst compounds, the most potent antiproliferative compound, **7l**, exhibited the lowest log *P* values and the highest TPSA, indicating the relevance of the latter physicochemical parameters to its highest activity. All tested compounds will likely be metabolised by CYP1A2, CYP2C19, and CYP2C9 but will be CYP2D3 inhibitors. However, only compounds **7k** and **7l** are considered substrates for CYP3A4. The predicted ADME properties are shown in (Table 7).

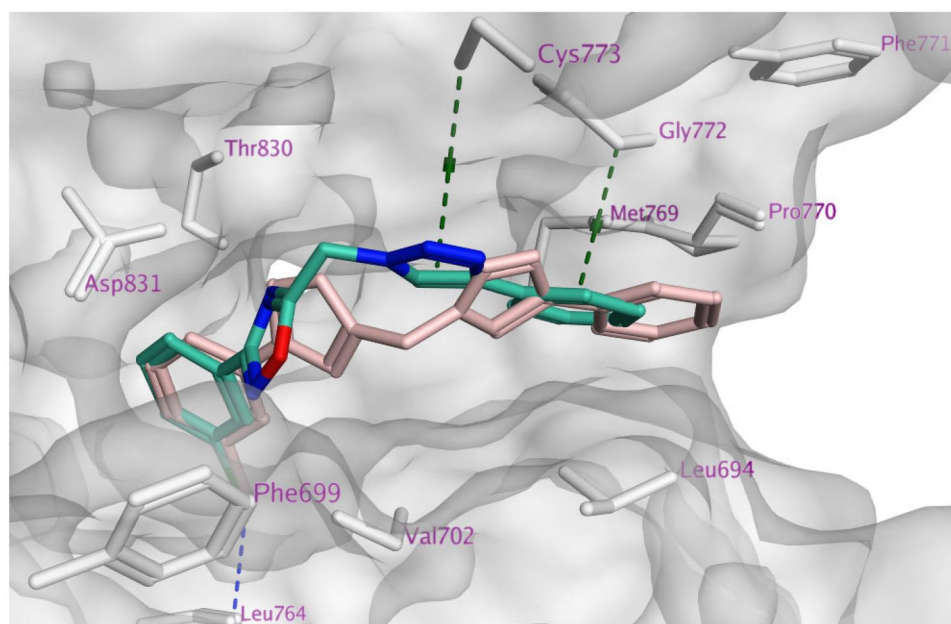
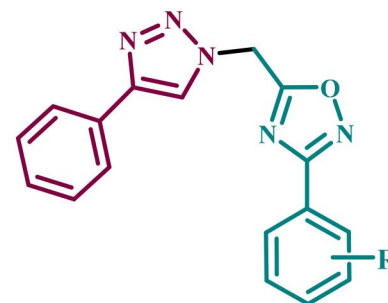
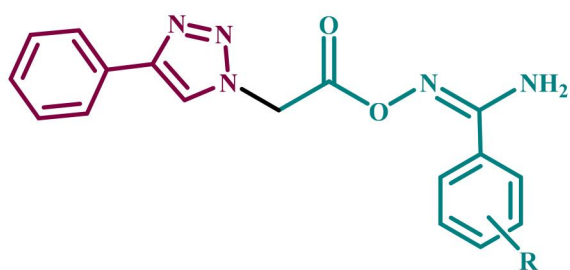


Figure 6. Docking representation model of compound **7h** (cyan) aligned with compound **7i** (pink) showing the protein surface (grey) of the site of EGFR (H-bond or halogen bond: blue dashed lines, Pi-H; green dashed lines).

Table 5. Ligand–protein complex interactions of the tested compounds **7h**, **7i**, **7j**, **7k**, and **7l** within the active site of VEGFR-2.

Compd.	MOE score (kcal/mol)	Hydrogen bond interactions	Hydrophobic interactions	Pi-H interactions
Sorafenib	−10.73	Cys919, Glu885	Val916, Leu889, Leu840, Asp1046, Cys1045 and Phe1047	Phe1047
7h	−8.24	Asp1046	Leu889, Leu840, Asp1046, Cys1045 and Phe1047	Lys868
7i	−8.11	Asp1046	Val916, Leu889, Leu840, Asp1046, Cys1045 and Phe1047	Leu840
7j	−7.92	Asp1046	Val916, Leu889, Leu840, Asp1046, Cys1045	Leu889, Lys868, Asp1046
7k	−8.71	Asp1046	Val916, Leu889, Leu840, Asp1046, Cys1045
7l	−9.10	Asp1046	Phe1047, Val916, Leu889, Leu840, Asp1046, Cys1045	Lys868, Leu840
				Lys868, Leu840

Structure activity relationship (SAR) analysis



Previously reported open chain compounds

(**6a-o**)

1. In general, cyclisation of amidoximes **6a-o** to 1,2,4-oxadiazole derivatives **7a-o** increased the activity of the newly synthesised compounds. The new 1,2,4-oxadiazole compounds are sterically fixed analogues of the open carboximidamide derivatives **6a-o**. Such a rigid conformation may result in tight fitting within the receptor active site.
2. The substitution on the phenyl group of the 1,2,4-oxadiazole moiety significantly increased the activity (except for methyl group) of **7a-o**, and substitution with methoxy groups increased the activity more than halogen atoms. Similar reasoning applies to the amidoxime derivatives **6a-o**, where

Newly synthesized cyclic chain compounds

(**7a-o**)

- substitution of the amidoxime moiety's phenyl group with electron donating or electron withdrawing groups' increases activity.
3. The number of methoxy groups substantially impacts the activity of **7a-o** compounds where the trimethoxy derivative > dimethoxy > mono-methoxy one. In **6a-o**, the dimethoxy derivative was the most tolerated for activity.
4. The type, position, and number of halogen atoms had a significant effect on antiproliferative activity of **7a-o**, with activity increasing in the order 2,4-di-Cl > 3-Br > 3-Cl > 4-Br > 4-Cl > 4-F. The dihalo derivative was also more active than

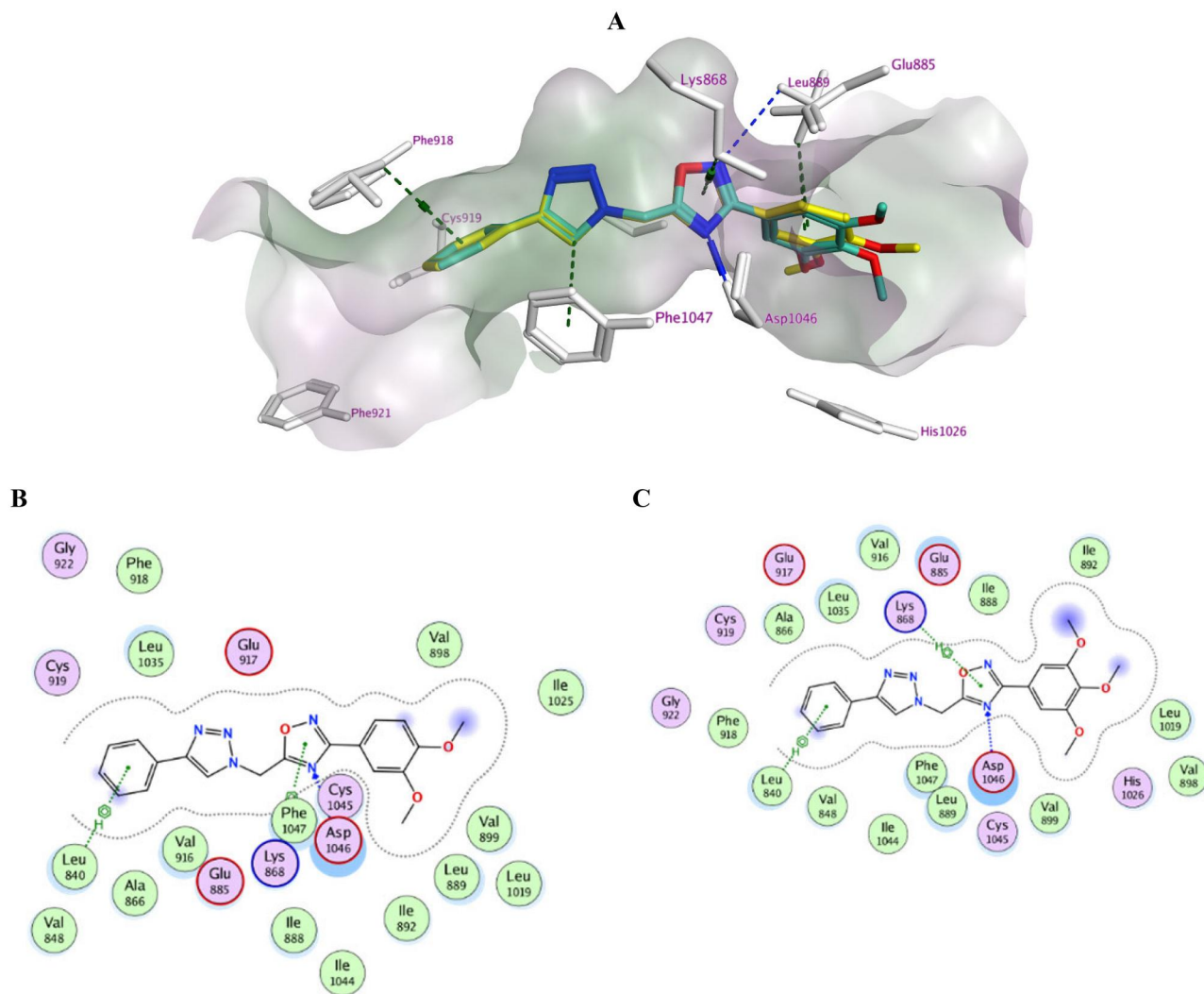


Figure 7. Docking representation model of compounds **7k** and **7l** within the binding site of VEGFR-2 (H-bond: blue dashed lines, Pi-H; green dashed lines). (A) 3D-docked model of compound **7k** (yellow) aligned with compound **7l** (cyan) showing the lipophilicity surface of active site (purple; hydrophilic, white; neutral; green; lipophilic); (B) 2D-docked model of compound **7k**; (C) 2D-docked model of compound **7l**.

the mono-halo derivative in **6a-o**, but the 4-position is better tolerated than the 3-position.

- When the phenyl group in **6a-o** and **7a-o** is replaced with a naphthalene moiety, the activity increases, and 1-naphthyl is tolerated better than 2-naphthyl.

Conclusion

Fifteen novel 1,2,3-triazole/1,2,4-oxadiazole hybrids (**7a-o**) were synthesised and tested as antiproliferative agents with dual EGFR/VEGFR-2 inhibitory activity. The newly synthesised compounds showed promising antiproliferative activity, with the hybrid **7h-l** being the most potent class. *In vitro* investigations revealed that compounds **7j**, **7k**, and **7l** were effective antiproliferative agents that could operate as dual EGFR/VEGFR-2 inhibitors. Moreover, apoptotic-inducing activity experiments indicate that compounds **7j**, **7k**, and **7l** enhance apoptosis by activating caspase-3, 8, and Bax and down-regulating the anti-apoptotic Bcl-2. Docking simulations highlighted the output of including 1,2,4-oxadiazole scaffold to improve the binding of the compounds within the active sites of EGFR and VEGFR-2. The cyclized structures fit well within the bioactive conformations. In addition, the phenyl triazole scaffold bound considerably within the hydrophobic pocket of binding sites.

Moreover, there is a future concern about introducing an H-bond forming substituent at the phenyl ring to tolerate binding with Cys919 within the VEGFR-2 active site. Also, docking results revealed that **7l** and **7k** exhibited the best binding mode within both active sites. *In silico* ADME and pharmacokinetic study, the compounds were predicted to have acceptable bioavailability and pharmacokinetic profiles.

Materials and methods

Chemistry

General details: see Appendix A

Compounds **1**, **2**, **5a-o**, and **6a-o** were prepared according to previously reported literature^{27,31-33}.

General procedures for the synthesis of compounds **7a-o**

A stirred solution of the appropriate *N'*-(((4-phenyl-1*H*-1,2,3-triazol-1-yl)acetyl)oxy)benzene-carboximidamide (**6a-o**) (0.78 mmole) in dry acetonitrile (20 mL) was refluxed overnight. After the reaction was completed (monitored with TLC), the excess solvent evaporated under reduced pressure. The obtained precipitate was washed with cold water, filtered, and crystallised from acetonitrile.

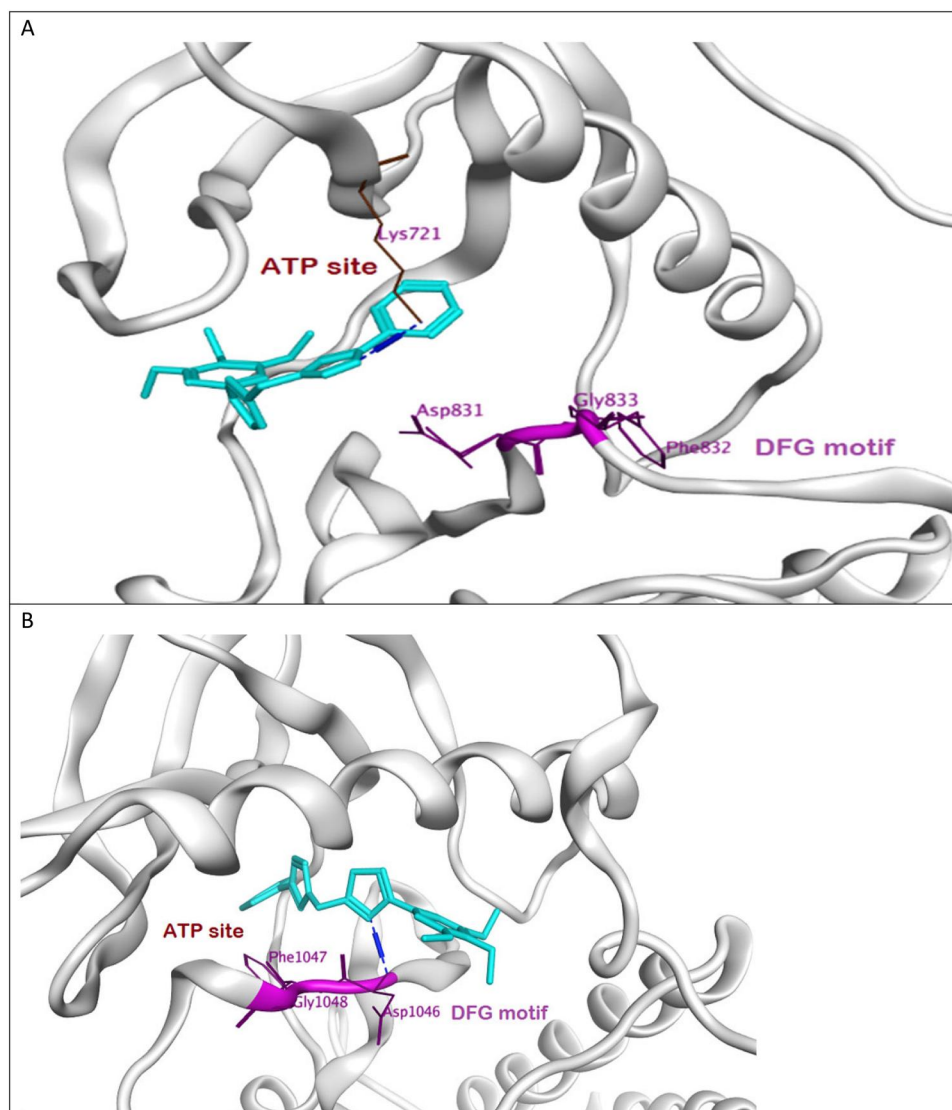


Figure 8. (A) Binding mode of compound 7i (cyan) to active site of EGFR showing DFG motif in purple. (B) Binding mode of compound 7i (cyan) to active site of VEGFR-2 showing DFG motif in purple.

Table 6. Physicochemical and pharmacokinetic properties (Lipinski parameters) of compounds 7h, 7i, 7j, 7k, and 7l.

Compd.	MW	ⁿ ROTB	HBA	HBD	Violations	MR	TPSA	log P
7h	338	4	5	0	0	89.5	70	3.33
7i	382	4	5	0	0	92.2	70	3.43
7j	372	4	5	0	0	94.5	70	3.85
7k	363	6	7	0	0	97.5	88	2.77
7l	393	7	8	0	0	103.9	97	2.76

3-Phenyl-5-[(4-phenyl-1H-1,2,3-triazol-1-yl)methyl]-1,2,4-oxadiazole (7a)⁴⁹

Yield: 0.19 g (78%), white solid, mp: 146–148 °C, *R*_f: 0.72 (hexane:ethyl acetate, 2:1, v/v). IR (FTIR): ν_{\max} (cm⁻¹) 3126, 3100, 2964 (CH), 1596, 1580, 1467 (C=N and C=C), 766 and 689 (Ar-CH bending). ¹H NMR (400 MHz, δ ppm DMSO-*d*₆): 8.81 (s, 1H, triazole-CH), 7.99 (d, *J* = 7.9 Hz, 2H, Ar-H), 7.90 (d, *J* = 8.5 Hz, 2H, Ar-H), 7.62–7.56 (m, 3H, Ar-H), 7.48 (t, *J* = 7.6 Hz, 2H, Ar-H), 7.37 (t, *J* = 7.4 Hz, 1H, Ar-H), 6.29 (s, 2H, N-CH₂). Anal. Calc. (%) for C₁₇H₁₃N₅O: C, 67.32; H, 4.32; N, 23.09. Found: C, 67.49; H, 4.60; N, 23.37.

3-(4-Fluorophenyl)-5-[(4-phenyl-1H-1,2,3-triazol-1-yl)methyl]-1,2,4-oxadiazole (7b)

Yield: 0.12 g (48%), white solid, mp: 137–139 °C, *R*_f: 0.74 (hexane:ethyl acetate, 2:1, v/v). IR (FTIR): ν_{\max} (cm⁻¹) 3125, 3099, 2979, 2952 (CH), 1608, 1578, 1469 (C=N and C=C), 848, 770, 700 (Ar-CH bending). ¹H NMR (400 MHz, δ ppm DMSO-*d*₆): 8.81 (s, 1H, triazole-CH), 8.05 (q, *J* = 4.8 Hz, 2H, Ar-H), 7.90 (d, *J* = 7.4 Hz, 2H, Ar-H), 7.48 (t, *J* = 7.4 Hz, 2H, Ar-H), 7.39 (q, *J* = 8.6 Hz, 3H, Ar-H), 6.30 (s, 2H, N-CH₂). ¹³C NMR (100 MHz, δ ppm DMSO-*d*₆): 175.1, 167.7, 166.2, 162.9, 147.3, 130.7, 130.2 (d, *J* = 9.2 Hz), 129.5, 128.6, 125.7, 123.1, 117.0 (d, *J* = 22.4 Hz), 45.5. Anal. Calc. (%) for C₁₇H₁₂FN₅O: C, 63.55; H, 3.76; N, 21.80. Found: C, 63.38; H, 3.91; N, 22.03.

3-(4-Chlorophenyl)-5-[(4-phenyl-1H-1,2,3-triazol-1-yl)methyl]-1,2,4-oxadiazole (7c)

Yield: 0.16 g (61%), white solid, mp: 150–152 °C, *R*_f: 0.71 (hexane:ethyl acetate, 2:1, v/v). IR (FTIR): ν_{\max} (cm⁻¹) 3137, 3086, 2977, 2957 (CH), 1598, 1569, 1467 (C=N and C=C), 844, 766, 697 (Ar-CH bending). ¹H NMR (400 MHz, δ ppm DMSO-*d*₆): 8.80 (s, 1H, triazole-CH), 8.00 (d, *J* = 8.5 Hz, 2H, Ar-H), 7.89 (d, *J* = 7.4 Hz, 2H, Ar-

Table 7. ADME properties of compounds **7h**, **7i**, **7j**, **7k**, and **7l**.

Compd.	GI abs.	BBB	P-gp substrate	CYP1A2 inhibitor	CYP2C19 inhibitor	CYP2C9 inhibitor	CYP2D6 inhibitor	CYP3A4 inhibitor
7h	High	Yes	No	Yes	Yes	Yes	No	No
7i	High	Yes	No	Yes	Yes	Yes	No	No
7j	High	Yes	No	Yes	Yes	Yes	No	No
7k	High	No	No	Yes	Yes	Yes	No	Yes
7l	High	No	No	Yes	Yes	Yes	No	Yes

H), 7.63 (d, $J=8.5$ Hz, 2H, Ar-H), 7.47 (t, $J=7.6$ Hz, 2H, Ar-H), 7.36 (t, $J=7.3$ Hz, 1H, Ar-H), 6.29 (s, 2H, N-CH₂). Anal. Calc. (%) for C₁₇H₁₂ClN₅O: C, 60.45; H, 3.58; N, 20.73. Found: C, 60.71; H, 3.69; N, 20.95.

3-(4-Bromophenyl)-5-[(4-phenyl-1H-1,2,3-triazol-1-yl)methyl]-1,2,4-oxadiazole (**7d**)

Yield: 0.22 g (74%), white solid, mp: 158–160 °C, R_f 0.73 (hexane:ethyl acetate, 2:1, v/v). IR (FTIR): ν_{\max} (cm⁻¹) 3122, 3093 (CH), 1592, 1564, 1459 (C=N and C=C), 838, 766, 697 (Ar-CH bending). ¹H NMR (400 MHz, δ ppm DMSO-*d*₆): 8.80 (s, 1H, triazole-CH), 7.92 (d, $J=8.6$ Hz, 2H, Ar-H), 7.90 (d, $J=7.1$ Hz, 2H, Ar-H), 7.78 (d, $J=8.6$ Hz, 2H, Ar-H), 7.48 (t, $J=7.7$ Hz, 2H, Ar-H), 7.37 (t, $J=7.5$ Hz, 1H, Ar-H), 6.29 (s, 2H, N-CH₂). Anal. Calc. (%) for C₁₇H₁₂BrN₅O: C, 53.42; H, 3.16; N, 18.32. Found: C, 53.66; H, 3.40; N, 18.59.

3-(4-Methylphenyl)-5-[(4-phenyl-1H-1,2,3-triazol-1-yl)methyl]-1,2,4-oxadiazole (**7e**)

Yield: 0.20 g (83%), white solid, mp: 140–142 °C, R_f 0.69 (hexane:ethyl acetate, 2:1, v/v). IR (FTIR): ν_{\max} (cm⁻¹) 3121, 3089, 2966, 2935 (CH), 1604, 1574, 1466 (C=N and C=C), 834, 769, 693 (Ar-CH bending). ¹H NMR (400 MHz, δ ppm DMSO-*d*₆): 8.81 (s, 1H, triazole-CH), 7.92–7.87 (m, 4H, Ar-H), 7.48 (d, $J=7.5$ Hz, 2H, Ar-H), 7.40–7.35 (m, 3H, Ar-H), 6.28 (s, 2H, N-CH₂), 2.38 (s, 3H, Ar-CH₃). ¹³C NMR (100 MHz, δ ppm DMSO-*d*₆): 174.7, 168.4, 147.3, 142.4, 130.7, 130.4, 129.5, 128.7, 127.5, 125.8, 123.3, 123.1, 45.6, 21.6. Anal. Calc. (%) for C₁₈H₁₅N₅O: C, 68.13; H, 4.76; N, 22.07. Found: C, 68.35; H, 4.88; N, 21.89.

3-(4-Methoxyphenyl)-5-[(4-phenyl-1H-1,2,3-triazol-1-yl)methyl]-1,2,4-oxadiazole (**7f**)

Yield: 0.19 g (75%), white solid, mp: 148–150 °C, R_f 0.70 (hexane:ethyl acetate, 2:1, v/v). IR (FTIR): ν_{\max} (cm⁻¹) 3133, 2977, 2843 (CH), 1617, 1576, 1469 (C=N and C=C), 843, 769, 698 (Ar-CH bending). ¹H NMR (400 MHz, δ ppm DMSO-*d*₆): 8.80 (s, 1H, triazole-CH), 7.93 (d, $J=8.9$ Hz, 2H, Ar-H), 7.90 (d, $J=7$ Hz, 2H, Ar-H), 7.48 (t, $J=7.5$ Hz, 2H, Ar-H), 7.37 (t, $J=7.4$ Hz, 1H, Ar-H), 7.11 (d, $J=8.9$ Hz, 2H, Ar-H), 6.26 (s, 2H, N-CH₂), 3.83 (s, 3H, Ar-OCH₃). Anal. Calc. (%) for C₁₈H₁₅N₅O₂: C, 64.86; H, 4.54; N, 21.01. Found: C, 65.08; H, 4.67; N, 21.28.

3-(4-Trifluoromethylphenyl)-5-[(4-phenyl-1H-1,2,3-triazol-1-yl)methyl]-1,2,4-oxadiazole (**7g**)

Yield: 0.13 g (46%), white solid, mp: 166–168 °C, R_f 0.7 (hexane:ethyl acetate, 2:1, v/v). IR (FTIR): ν_{\max} (cm⁻¹) 3144, 3001, 2965 (CH), 1602, 1579, 1468 (C=N and C=C), 856, 767, 694 (Ar-CH bending). ¹H NMR (400 MHz, δ ppm DMSO-*d*₆): 8.82 (s, 1H, triazole-CH), 8.21 (d, $J=8.1$ Hz, 2H, Ar-H), 7.94 (d, $J=8.4$ Hz, 2H, Ar-H), 7.90 (d, $J=7.5$ Hz, 2H, Ar-H), 7.48 (t, $J=7.5$ Hz, 2H, Ar-H), 7.37 (t, $J=7.3$ Hz, 1H, Ar-H), 6.33 (s, 2H, N-CH₂). ¹³C NMR (100 MHz, δ

ppm DMSO-*d*₆): 175.1, 167.2, 147.1, 131.8 (q, $J=32.2$ Hz), 130.3, 129.6, 129.2, 128.4, 128.2, 126.5 (q, $J=3.5$ Hz), 125.5, 124.0 (q, $J=27.27$ Hz), 122.9, 45.3. Anal. Calc. (%) for C₁₈H₁₂F₃N₅O: C, 58.22; H, 3.26; N, 18.86. Found: C, 58.43; H, 3.39; N, 19.07.

3-(3-Chlorophenyl)-5-[(4-phenyl-1H-1,2,3-triazol-1-yl)methyl]-1,2,4-oxadiazole (**7h**)

Yield: 0.17 g (67%), white solid, mp: 128–130 °C, R_f 0.71 (hexane:ethyl acetate, 2:1, v/v). IR (FTIR): ν_{\max} (cm⁻¹) 3121, 3095, 2966 (CH), 1606, 1574, 1465 (C=N and C=C), 892, 796, 767, 736, 693 (Ar-CH bending). ¹H NMR (400 MHz, δ ppm DMSO-*d*₆): 8.80 (s, 1H, triazole-CH), 7.97–7.94 (m, 2H, Ar-H), 7.89 (d, $J=7.3$ Hz, 2H, Ar-H), 7.69 (d, $J=8.7$ Hz, 1H, Ar-H), 7.60 (t, $J=8.1$ Hz, 1H, Ar-H), 7.47 (t, $J=7.6$ Hz, 2H, Ar-H), 7.37 (t, $J=7.3$ Hz, 1H, Ar-H), 6.30 (s, 2H, N-CH₂). ¹³C NMR (100 MHz, δ ppm DMSO-*d*₆): 174.8, 167.0, 146.9, 134.0, 131.8, 131.5, 130.2, 129.0, 128.2, 127.5, 126.5, 125.8, 125.3, 122.7, 45.1. Anal. Calc. (%) for C₁₇H₁₂ClN₅O: C, 60.45; H, 3.58; N, 20.73. Found: C, 60.72; H, 3.79; N, 21.01.

3-(3-Bromophenyl)-5-[(4-phenyl-1H-1,2,3-triazol-1-yl)methyl]-1,2,4-oxadiazole (**7i**)

Yield: 0.23 g (77%), white solid, mp: 139–141 °C, R_f 0.72 (hexane:ethyl acetate, 2:1, v/v). IR (FTIR): ν_{\max} (cm⁻¹) 3143, 3067, 3002 (CH), 1595, 1564, 1471 (C=N and C=C), 903, 800, 767, 737, 694 (Ar-CH bending). ¹H NMR (400 MHz, δ ppm DMSO-*d*₆): 8.80 (s, 1H, triazole-CH), 8.10 (t, $J=1.7$ Hz, 1H, Ar-H), 7.99 (two t, $J=8, 2.5$ Hz, 1H, Ar-H), 7.89 (d, $J=7.1$ Hz, 2H, Ar-H), 7.84–7.80 (m, 1H, Ar-H), 7.54 (t, $J=7.9$ Hz, 1H, Ar-H), 7.48 (t, $J=7.5$ Hz, 2H, Ar-H), 7.37 (t, $J=7.4$ Hz, 1H, Ar-H), 6.30 (s, 2H, N-CH₂). Anal. Calc. (%) for C₁₇H₁₂BrN₅O: C, 53.42; H, 3.16; N, 18.32. Found: C, 53.68; H, 3.29; N, 18.57.

3-(2,4-Dichlorophenyl)-5-[(4-phenyl-1H-1,2,3-triazol-1-yl)methyl]-1,2,4-oxadiazole (**7j**)

Yield: 0.16 g (54%), white solid, mp: 137–139 °C, R_f 0.73 (hexane:ethyl acetate, 2:1, v/v). IR (FTIR): ν_{\max} (cm⁻¹) 3146, 3080, 2992 (CH), 1602, 1588, 1469 (C=N and C=C), 881, 762, 690 (Ar-CH bending). ¹H NMR (400 MHz, δ ppm DMSO-*d*₆): 8.80 (s, 1H, triazole-CH), 7.93–7.88 (m, 4H, Ar-H), 7.64 (two d, $J=8.4, 2.1$ Hz, 1H, Ar-H), 7.48 (t, $J=8.4$ Hz, 2H, Ar-H), 7.37 (t, $J=7.4$ Hz, 1H, Ar-H), 6.32 (s, 2H, N-CH₂). ¹³C NMR (100 MHz, δ ppm DMSO-*d*₆): 174.1, 166.0, 146.9, 136.8, 133.2, 133.0, 130.6, 130.2, 129.0, 128.2, 128.1, 125.3, 123.8, 122.7, 45.0. Anal. Calc. (%) C₁₇H₁₁Cl₂N₅O: C, 54.86; H, 2.98; N, 18.82. Found: C, 54.98; H, 3.12; N, 19.09.

3-(3,4-Dimethoxyphenyl)-5-[(4-phenyl-1H-1,2,3-triazol-1-yl)methyl]-1,2,4-oxadiazole (**7k**)

Yield: 0.25 g (89%), white solid, mp: 174–176 °C, R_f 0.68 (hexane:ethyl acetate, 2:1, v/v). IR (FTIR): ν_{\max} (cm⁻¹) 3125, 3096, 2943, 2838 (CH), 1601, 1583, 1499 (C=N and C=C), 864, 765, 687 (Ar-CH bending). ¹H NMR (400 MHz, δ ppm DMSO-*d*₆): 8.80 (s, 1H,

triazole-CH), 7.89 (d, $J = 7.3$ Hz, 2H, Ar-H), 7.57 (two d, $J = 8.4$, 1.8 Hz, 1H, Ar-H), 7.49–7.45 (m, 3H, Ar-H), 7.36 (t, $J = 7.3$ Hz, 1H, Ar-H), 7.11 (d, $J = 8.5$ Hz, 1H, Ar-H), 6.26 (s, 2H, N-CH₂), 3.82 (s, 6H, Ar-(OCH₃)₂). ¹³C NMR (100 MHz, δ ppm DMSO-*d*₆): 174.0, 167.8, 151.7, 149.1, 146.9, 130.3, 129.0, 128.2, 125.3, 122.7, 120.7, 117.8, 112.0, 109.5, 55.7, 55.6, 45.1. Anal. Calc. (%) C₁₉H₁₇N₅O₃: C, 62.80; H, 4.72; N, 19.27. Found: C, 62.67; H, 4.89; N, 19.51.

3-(3,4,5-Trimethoxyphenyl)-5-[(4-phenyl-1H-1,2,3-triazol-1-yl)methyl]-1,2,4-oxadiazole (7l)

Yield: 0.21 g (69%), white solid, mp: 154–156 °C, R_f : 0.74 (hexane:ethyl acetate, 2:1, v/v). IR (FTIR): ν_{\max} (cm⁻¹) 3143, 3000, 2947, 2847 (CH), 1604, 1581, 1467 (C=N and C=C), 762, 689 (Ar-CH bending). ¹H NMR (400 MHz, δ ppm DMSO-*d*₆): 8.81 (s, 1H, triazole-CH), 7.89 (d, $J = 7$ Hz, 2H, Ar-H), 7.48 (t, $J = 7.5$ Hz, 2H, Ar-H), 7.37 (t, $J = 7.4$ Hz, 1H, Ar-H), 7.26 (s, 2H, Ar-H), 6.27 (s, 2H, N-CH₂), 3.85 (s, 6H, Ar-(OCH₃)₂), 3.74 (s, 3H, Ar-OCH₃). Anal. Calc. (%) C₂₀H₁₉N₅O₄: C, 61.06; H, 4.87; N, 17.80. Found: C, 61.28; H, 4.95; N, 18.04.

3-(Naphthalen-1-yl)-5-[(4-phenyl-1H-1,2,3-triazol-1-yl)methyl]-1,2,4-oxadiazole (7m)

Yield: 0.21 g (78%), white solid, mp: 144–146 °C, R_f : 0.69 (hexane:ethyl acetate, 2:1, v/v). IR (FTIR): ν_{\max} (cm⁻¹) 3120, 3088, 2975, 2943 (CH), 1607, 1592, 1464 (C=N and C=C), 767, 747, 694 (Ar-CH bending). ¹H NMR (400 MHz, δ ppm DMSO-*d*₆): 8.86 (s, 1H, triazole-CH), 8.76 (d, $J = 8.3$ Hz, 1H, Ar-H), 8.19 (d, $J = 7.7$ Hz, 2H, Ar-H), 8.08 (d, $J = 7.9$ Hz, 1H, Ar-H), 7.91 (d, $J = 7.2$ Hz, 2H, Ar-H), 7.72–7.63 (m, 3H, Ar-H), 7.48 (t, $J = 7.5$ Hz, 2H, Ar-H), 7.37 (t, $J = 7.3$ Hz, 1H, Ar-H), 6.37 (s, 2H, N-CH₂). ¹³C NMR (100 MHz, δ ppm DMSO-*d*₆): 173.6, 168.3, 146.9, 133.5, 132.3, 130.3, 129.7, 129.5, 129.0, 128.9, 128.2, 127.9, 126.7, 125.5, 125.4, 125.3, 122.7, 122.5, 45.2. Anal. Calc. (%) C₂₁H₁₅N₅O: C, 71.38; H, 4.28; N, 19.82. Found: C, 71.09; H, 4.41; N, 20.04.

3-(Naphthalen-2-yl)-5-[(4-phenyl-1H-1,2,3-triazol-1-yl)methyl]-1,2,4-oxadiazole (7n)

Yield: 0.23 g (84%), white solid, mp: 180–182 °C, R_f : 0.66 (hexane:ethyl acetate, 2:1, v/v). IR (FTIR): ν_{\max} (cm⁻¹) 3117, 3088, 2971, 2939 (CH), 1600, 1462 (C=N and C=C), 764, 756, 689 (Ar-CH bending). ¹H NMR (400 MHz, δ ppm DMSO-*d*₆): 8.81 (s, 1H, triazole-CH), 8.61 (s, 1H, Ar-H), 8.12 (d, $J = 7.8$ Hz, 1H, Ar-H), 8.06 (t, $J = 7.5$ Hz, 2H, Ar-H), 8.00 (d, $J = 7.8$ Hz, 1H, Ar-H), 7.91 (d, $J = 7.9$ Hz, 2H, Ar-H), 7.66–7.59 (m, 2H, Ar-H), 7.48 (t, $J = 7.6$ Hz, 2H, Ar-H), 7.37 (t, $J = 7.4$ Hz, 1H, Ar-H), 6.31 (s, 2H, N-CH₂). Anal. Calc. (%) C₂₁H₁₅N₅O: C, 71.38; H, 4.28; N, 19.82. Found: C, 71.21; H, 4.52; N, 20.06.

3-(2H-1,3-Benzodioxol-5-yl)-5-[(4-phenyl-1H-1,2,3-triazol-1-yl)methyl]-1,2,4-oxadiazole (7o)

Yield: 0.18 g (67%), white solid, mp: 149–151 °C, R_f : 0.67 (hexane:ethyl acetate, 2:1, v/v). IR (FTIR): ν_{\max} (cm⁻¹) 3141, 2982, 2914 (CH), 1583, 1452 (C=N and C=C), 761, 692 (Ar-CH bending). ¹H NMR (400 MHz, δ ppm DMSO-*d*₆): 8.80 (s, 1H, triazole-CH), 7.89 (d, $J = 7.1$ Hz, 2H, Ar-H), 7.55 (two d, $J = 8.13$, 1.7 Hz, 1H, Ar-H), 7.48 (d, $J = 7.6$ Hz, 2H, Ar-H), 7.43 (d, $J = 1.6$ Hz, 1H, Ar-H), 7.37 (t, $J = 7.4$ Hz, 1H, Ar-H), 7.08 (d, $J = 8.13$ Hz, 1H, Ar-H), 6.25 (s, 2H, -O-CH₂-O-), 6.14 (s, 2H, N-CH₂). ¹³C NMR (100 MHz, δ ppm DMSO-*d*₆): 174.1, 167.6, 150.3, 148.1, 146.9, 130.3, 129.0, 128.2,

125.3, 122.7, 122.3, 119.2, 109.0, 106.5, 102.0, 45.1. Anal. Calc. (%) C₁₈H₁₃N₅O₃: C, 62.24; H, 3.77; N, 20.16. Found: C, 62.45; H, 3.85; N, 20.42.

Biology

Assay of cell viability effect

To investigate the effect of compounds **7a–o** on normal cell lines, a cell viability experiment was performed on the MCF-10A (human mammary gland epithelial) cell line. This experiment uses 50 μ M of the investigated compound for four days^{34,35}. Refer to Appendix A (Supp. File) for more details.

Assay of antiproliferative effect

The antiproliferative activity of 1,2,4-oxadiazoles **7a–o** against four human cancer cell lines was assessed using Erlotinib as the reference medication^{36,37}. See Appendix A for more details.

Assay of EGFR inhibitory activity

The inhibitory effects of the most potent antiproliferative compounds **7h–l** on EGFR, as a potential target for their antiproliferative action, were studied using Erlotinib as a control medication³⁸. For more information, see Appendix A.

Assay of VEGFR-2 inhibitory activity

Compounds **7h–l**'s inhibitory activity against VEGFR-2 was assessed using kinase-glo-luminescent kinase assays with Sorafenib as the control drug³⁹. For more information, see Appendix A.

Apoptosis-inducing activity assay

Compounds **7j**, **7k**, and **7l**, the most potent derivatives in all *in vitro* studies, were tested for their capacity to initiate the apoptosis cascade and reveal their proapoptotic potential⁴⁵. For more information, see Appendix A.

Docking

All molecular modelling calculations and docking simulation studies were performed on a Processor Intel (R) Pentium (R) CPU N3510@ 1.99 GHz and 4 GB memory with Microsoft Windows 8.1 pro (64 Bit) operating system using Molecular Operating Environment (MOE 2019.0102, 2020; Chemical Computing Group, Canada) as the computational software. MOE minimizations were performed until an RMSD gradient of 0.01 kcal/mol/Å with the force field (OPLS-AA) to calculate the partial charges automatically using Born solvation. Before simulations, the protein was corrected, hydrogens were added, and ionisation states were assigned; the system was optimised *via* protonation, distant water molecules were deleted, and the receptor was minimised using the QuickPrep function. Then, both ligand and pocket were isolated in 3D, and molecular surface was drawn around the binding site to visualise the space available for docked ligands. The compounds' database was created after the compounds' structures were prepared, partially charged, and minimised. Initially, self-docking was performed, and ligand conformations were generated with the bond rotation method. These are then placed on the site with the Triangle Matcher method and ranked with the London dG scoring function. The retain option specifies the number of poses (30) to pass to the refinement for energy minimisation in

the pocket before restoring with the GBVI/WSA dG scoring function. Docking simulation was performed using a compound database mdb file. A triangle matching with London dG scoring was chosen for initial placement, and then the top 30 poses were refined using force field (OPLS-AA) and GBVI/WSA dG scoring. The output database dock file was created with different poses for each ligand and arranged according to the final score function (S), which is the score of the last stage that was not set to zero.

Disclosure statement

The author reported no potential conflicts of interests.

Acknowledgements

This work was funded by the Researchers Supporting Project Number [RSP2023R273] at King Saud University, Riyadh, Saudi Arabia. The authors also acknowledge support from the KIT-Publication Fund of the Karlsruhe Institute of Technology.

References

1. Akram M, Iqbal M, Daniyal M, Khan AU. Awareness and current knowledge of breast cancer. *Biol Res.* 2017;50(1):33.
2. Youssif BGM, Abdelrahman MH, Abdelazeem AH, Abdelgawad MA, Ibrahim HM, Salem OIA, Mohamed MFA, Treambleau L, Bukhari SNA. Design, synthesis, mechanistic and histopathological studies of small-molecules of novel indole-2-carboxamides and pyrazino[1,2-a]indol-1 (2H)-ones as potential anticancer agents effecting the reactive oxygen species production. *Eur J Med Chem.* 2018;146:260–273.
3. Guo YJ, Pan WW, Liu SB, Shen ZF, Xu Y, Hu LL. ERK/MAPK signalling pathway and tumorigenesis. *Exp Ther Med.* 2020;19(3):1997–2007.
4. Zwick E, Bange J, Ullrich A. Receptor tyrosine kinase signalling as a target for cancer intervention strategies. *Endocr Relat Cancer.* 2001;8(3):161–173.
5. Huang L, Fu L. Mechanisms of resistance to EGFR tyrosine kinase inhibitors. *Acta Pharm Sin B.* 2015;5(5):390–401.
6. Yewale C, Baradia D, Vhora I, Patil S, Misra A. Epidermal growth factor receptor targeting in cancer: a review of trends and strategies. *Biomaterials.* 2013;34(34):8690–8707.
7. Mohamed FA, Gomaa HA, Hendawy O, Ali AT, Farghaly HS, Gouda AM, Abdelazeem AH, Abdelrahman MH, Trembleau L, Youssif BG. Design, synthesis, and biological evaluation of novel EGFR inhibitors containing 5-chloro-3-hydroxymethyl-indole-2-carboxamide scaffold with apoptotic antiproliferative activity. *Bioorg Chem.* 2021;112:104960.
8. Modi SJ, Kulkarni VM. Vascular endothelial growth factor receptor (VEGFR-2)/KDR inhibitors: medicinal chemistry perspective. *Med Drug Discov.* 2019;2:100009.
9. Falcon BL, Chintharlapalli S, Uhlik MT, Pytowski B. Antagonist antibodies to vascular endothelial growth factor receptor 2 (VEGFR-2) as anti-angiogenic agents. *Pharmacol Ther.* 2016;164:204–225.
10. Peng F-W, Liu D-K, Zhang Q-W, Xu Y-G, Shi L. VEGFR-2 inhibitors and the therapeutic applications thereof: a patent review (2012–2016). *Expert Opin Ther Pat.* 2017;27(9):987–1004.
11. Lemmon MA, Schlessinger J. Cell signaling by receptor tyrosine kinases. *Cell.* 2010;141(7):1117–1134.
12. Liao JJ-L. Molecular recognition of protein kinase binding pockets for design of potent and selective kinase inhibitors. *J Med Chem.* 2007;50(3):409–424.
13. Wheler JJ, Janku F, Naing A, Li Y, Stephen B, Zinner R, Subbiah V, Fu S, Karp D, Falchook GS, et al. TP53 alterations correlate with response to VEGF/VEGFR inhibitors: implications for targeted therapeutics. *Mol Cancer Ther.* 2016;15(10):2475–2485.
14. Xie C, Wan X, Quan H, Zheng M, Fu L, Li Y, Lou L. Preclinical characterization of anlotinib, a highly potent and selective vascular endothelial growth factor receptor-2 inhibitor. *Cancer Sci.* 2018;109(4):1207–1219.
15. Liu Z-L, Chen H-H, Zheng L-L, Sun L-P, Shi L. Angiogenic signaling pathways and anti-angiogenic therapy for cancer. *Signal Transduct Target Ther.* 2023;8(1):198.
16. Sun S, Zhang J, Wang N, Kong X, Fu F, Wang H, Yao J. Design and discovery of quinazoline- and thiourea-containing sorafenib analogs as EGFR and VEGFR-2 dual TK inhibitors. *Molecules.* 2017;23(1):24.
17. Liu X-J, Zhao H-C, Hou S-J, Zhang H-J, Cheng L, Yuan S, Zhang L-R, Song J, Zhang S-Y, Chen S-W. Recent development of multi-target VEGFR-2 inhibitors for the cancer therapy. *Bioorg Chem.* 2023;133:106425.
18. Farghaly TA, Al-Hasani WA, Abdulwahab HG. An updated patent review of VEGFR-2 inhibitors (2017–present). *Expert Opin Ther Pat.* 2021;31(11):989–1007.
19. Zhang H-Q, Gong F-H, Li C-G, Zhang C, Wang Y-J, Xu Y-G, Sun L-P. Design and discovery of 4-anilinoquinazoline-acylamino derivatives as EGFR and VEGFR-2 dual TK inhibitors. *Eur J Med Chem.* 2016;109:371–379.
20. Biernacki K, Daško M, Ciupak O, Kubiński K, Rachon J, Demkowicz S. Novel 1,2,4-oxadiazole derivatives in drug discovery. *Pharmaceuticals.* 2020;13(6):111.
21. Wang J-J, Sun W, Jia W-D, Bian M, Yu L-J. Research progress on the synthesis and pharmacology of 1,3,4-oxadiazole and 1,2,4-oxadiazole derivatives: a mini review. *J Enzyme Inhib Med Chem.* 2022;37(1):2304–2319.
22. Coupar I, Hedges A, Metcalfe HL, Turner P. Effect of aminophylline, butalamine and imolamine on human isolated smooth muscle. *J Pharm Pharmacol.* 1969;21(7):474–475.
23. Rotbart HA, Webster AD, Group PTR, Pleconaril Treatment Registry Group. Treatment of potentially life-threatening enterovirus infections with pleconaril. *Clin Infect Dis.* 2001;32(2):228–235.
24. McDonald CM, Campbell C, Torricelli RE, Finkel RS, Flanigan KM, Goemans N, Heydemann P, Kaminska A, Kirschner J, Muntoni F, Clinical Evaluator Training Group; ACT DMD Study Group, et al. Ataluren in patients with nonsense mutation Duchenne muscular dystrophy (ACT DMD): a multicentre, randomised, double-blind, placebo-controlled, phase 3 trial. *Lancet.* 2017;390(10101):1489–1498.
25. Dokla EM, Fang C-S, Abouzid KA, Chen CS. 1,2,4-Oxadiazole derivatives targeting EGFR and c-Met degradation in TKI resistant NSCLC. *Eur J Med Chem.* 2019;182:111607.
26. Venu K, Saritha B, Sailaja BBV. New molecular hybrids containing benzimidazole, thiazolidine-2,4-dione and 1,2,4-oxadiazole as EGFR directing cytotoxic agents. *Tetrahedron.* 2022;124:132991.
27. Mahmoud MA, Mohammed AF, Salem OI, Rabea SM, Youssif BG. Design, synthesis, and antiproliferative properties of new 1,2,3-triazole-carboximidamide derivatives as dual EGFR/VEGFR-2 inhibitors. *J Mol Struct.* 2023;1282:135165.

28. Al-Wahaibi LH, Mahmoud MA, Mostafa YA, Raslan AE, Youssif BG. Novel piperine-carboximidamide hybrids: design, synthesis, and antiproliferative activity via a multi-targeted inhibitory pathway. *J Enzyme Inhib Med Chem.* 2023;38 (1): 376–386.
29. Al-Wahaibi LH, Mohammed AF, Abdel Rahman FE-ZS, Abdelrahman MH, Gu X, Trembleau L, Youssif BG. Design, synthesis, apoptotic, and antiproliferative effects of 5-chloro-3-(2-methoxyvinyl)-indole-2-carboxamides and pyrido[3,4-b]indol-1-ones as potent EGFRWT/EGFRT790M inhibitors. *J Enzyme Inhib Med Chem.* 2023;38(1):2218602.
30. El-Sherief EM, Bräse S, Tawfeek HN, Alasmay FA, Youssif BG. Synthesis, antioxidant and antiproliferative actions of 4-(1,2,3-triazol-1-yl)quinolin-2 (1H)-ones as multi-target inhibitors. *Int J Mol Sci.* 2023;24(17):13300.
31. Abdu-Allah HH, Youssif BG, Abdelrahman MH, Abdel-Hamid MK, Reshma RS, Yogeewari P, Aboul-Fadl T, Sriram D. Synthesis and anti-mycobacterial activity of 4-(4-phenyl-1H-1,2,3-triazol-1-yl)salicylhydrazones: revitalizing an old drug. *Arch Pharm Res.* 2017;40(2):168–179.
32. Talukdar S, Hsu J-L, Chou T-C, Fang J-M. Direct transformation of aldehydes to nitriles using iodine in ammonia water. *Tetrahedron Lett.* 2001;42(6):1103–1105.
33. Frejat FOA, Zhai H, Cao Y, Wang L, Mostafa YA, Gomaa HA, Youssif BG, Wu C. Novel indazole derivatives as potent apoptotic antiproliferative agents by multi-targeted mechanism: synthesis and biological evaluation. *Bioorg Chem.* 2022; 126:105922.
34. Gomaa HAM, Shaker ME, Alzarea SI, Hendawy OM, Mohamed FAM, Gouda AM, Ali AT, Morcoss MM, Abdelrahman MH, Trembleau L, et al. Optimization and SAR investigation of novel 2,3-dihydropyrazino[1,2-a]indole-1,4-dione derivatives as EGFR and BRAFV600E dual inhibitors with potent antiproliferative and antioxidant activities. *Bioorg Chem.* 2022;120:105616.
35. Gomaa HA, El-Sherief HA, Hussein S, Gouda AM, Salem OI, Alharbi KS, Hayallah AM, Youssif BG. Novel 1,2,4-triazole derivatives as apoptotic inducers targeting p53: synthesis and antiproliferative activity. *Bioorg Chem.* 2020;105:104369.
36. Youssif BG, Gouda AM, Moustafa AH, Abdelhamid AA, Gomaa HA, Kamal I, Marzouk AA. Design and synthesis of new triarylimidazole derivatives as dual inhibitors of BRAFV600E/p38 α with potential antiproliferative activity. *J Mol Struct.* 2022;1253:132218.
37. Mekheimer RA, Allam SMR, Al-Sheikh MA, Moustafa MS, Al-Mousawi SM, Mostafa YA, Youssif BGM, Gomaa HAM, Hayallah AM, Abdelaziz M, et al. Discovery of new pyrimido[5,4-c]quinolines as potential antiproliferative agents with multitarget actions: rapid synthesis, docking, and ADME studies. *Bioorg Chem.* 2022;121:105693.
38. Mahmoud MA, Mohammed AF, Salem OI, Gomaa HA, Youssif BG. New 1,3,4-oxadiazoles linked with the 1,2,3-triazole moiety as antiproliferative agents targeting the EGFR tyrosine kinase. *Arch Pharm (Weinheim).* 2022;355(6):e2200009.
39. Marzouk AA, Abdel-Aziz SA, Abdelrahman KS, Wanas AS, Gouda AM, Youssif BG, Abdel-Aziz M. Design and synthesis of new 1,6-dihydropyrimidin-2-thio derivatives targeting VEGFR-2: molecular docking and antiproliferative evaluation. *Bioorg Chem.* 2020;102:104090.
40. Liu Y, Zhu X. Endoplasmic reticulum-mitochondria tethering in neurodegenerative diseases. *Transl Neurodegener.* 2017; 6(1):21.
41. Villa-Pulgarín JA, Gajate C, Botet J, Jimenez A, Justies N, Varela-M RE, Cuesta-Marbán Á, Müller I, Modolell M, Revuelta JL, et al. Mitochondria and lipid raft-located FOF1-ATP synthase as major therapeutic targets in the antileishmanial and anticancer activities of ether lipid edelfosine. *PLoS Negl Trop Dis.* 2017;11(8):e0005805.
42. Bao H, Zhang Q, Zhu Z, Xu H, Ding F, Wang M, Du S, Du Y, Yan Z. BHX, a novel pyrazoline derivative, inhibits breast cancer cell invasion by reversing the epithelial-mesenchymal transition and down-regulating Wnt/ β -catenin signaling. *Sci Rep.* 2017;7(1):9153.
43. Al-Wahaibi LH, Mostafa YA, Abdelrahman MH, El-Bahrawy AH, Trembleau L, Youssif BG. Synthesis and biological evaluation of indole-2-carboxamides with potent apoptotic antiproliferative activity as EGFR/CDK2 dual inhibitors. *Pharmaceuticals.* 2022;15(8):1006.
44. Choudhary GS, Al-Harbi S, Almasan A. Caspase-3 activation is a critical determinant of genotoxic stress-induced apoptosis. *Methods Mol Biol.* 2015;1219:1–9.
45. Youssif BG, Mohamed AM, Osman EEA, Abou-Ghadir OF, Elnaggar DH, Abdelrahman MH, Treambul L, Gomaa HA. 5-Chlorobenzofuran-2-carboxamides: from allosteric CB1 modulators to potential apoptotic antitumor agents. *Eur J Med Chem.* 2019;177:1–11.
46. Shattuck TW. Colby college molecular mechanics exercises MOE (molecular operating environment) exercises. Montreal, QC: Chemical Computing Group ULC; 2011.
47. McTigue M, Murray BW, Chen JH, Deng Y-L, Solowiej J, Kania RS. Molecular conformations, interactions, and properties associated with drug efficiency and clinical performance among VEGFR TK inhibitors. *Proc Natl Acad Sci U S A.* 2012; 109(45):18281–18289.
48. Daina A, Michielin O, Zoete VJ. SwissADME: a free web tool to evaluate pharmacokinetics, drug-likeness and medicinal chemistry friendliness of small molecules. *Sci Rep.* 2017;7(1): 42717.
49. Pokhodylo NT, Savka RD, Shyyka OY, Obushak MD. One-pot CuAAC synthesis of (1H-1,2,3-triazol-1-yl) methyl-1,3,4/1,2,4-oxadiazoles starting from available chloromethyl-1,3,4/1,2,4-oxadiazoles. *J Heterocycl Chem.* 2020;57(7):2969–2976.